CHEMBIOCHEM

DOI: 10.1002/cbic.200700009

Determination of the Conformation of the Human VDAC1 N-Terminal Peptide, a Protein Moiety Essential for the Functional Properties of the Pore

Vito De Pinto,*[a] Flora Tomasello,[a] Angela Messina,[a] Francesca Guarino,[a] Roland Benz,[b] Diego La Mendola,[c] Antonio Magrì,[c] Danilo Milardi,[c] and Giuseppe Pappalardo*[c]

*Mitochondrial porin or VDAC (voltage-dependent anion-selective channel) is the most abundant protein in the mitochondrial outer membrane. The structure of VDAC has been predicted to be a transmembrane β-barrel with an α-helix at the N terminus. It is a matter of debate as to whether this putative α-helix plays a structural role as a component of the pore walls or a function in the pore activity. We have synthesised the human VDAC1 (HVDAC1) N-terminal peptide Ac-AVPPTYADLGKSARDVFTK-NH_2 (**Prn2–20**) and determined its structure by CD and NMR spectroscopy. CD studies show that the **Prn2–20** peptide exists in aqueous solvent as an unstructured peptide with no stable secondary structure. In membrane-mimetic SDS micelles or water/trifluoroethanol, however, it assumes an amphipathic α-helix conformation between Tyr5 and Val16, as deduced from NMR. No ordered structure was observed in dodecyl β-maltoside. Differential scanning calorimetric measurements were carried out in order to examine the membrane affinity of the peptide. Upon interaction with the negatively charged 1,2 dipalmitoyl-sn-glycero-3-phosphoserine membrane, **Prn2–20** exhibited distinctive behaviour, suggesting that electrostatics play an important role. Interaction between the peptide and artificial bilayers indicates that the peptide lies on the membrane surface. Recombinant HVDAC1 deletion mutants, devoid of seven or 19 N-terminal amino acids, were used for transfection of eukaryotic cells. Over-expression of HVDAC1 increases the number of Cos cells with depolarised mitochondria, and this effect is progressively reduced in cells transfected with HVDAC1 lacking those seven or 19 amino acids. The mitochondrial targeting of the deletion mutants is unaffected. The overall picture emerging from our experiments is that the VDAC N-terminal peptide plays a role in the proper function of this protein during apoptotic events.*

Introduction

Voltage-dependent anion channel (VDAC1, also known as mitochondrial porin) is an integral membrane protein with a molecular mass of 30–32 kDa[1–4] and is the most abundant protein found in the outer mitochondrial membranes of all eukaryotes, constituting up to 50% of the protein embedded in this membrane in *Neurospora crassa*.[5] This transmembrane pore-forming protein is an efficient molecular filter for hydrophilic solutes up to a well defined exclusion limit of about 3000–5000 Da in the mitochondrial outer membrane.[1–4,6] VDACs have conserved sequences with lengths of about 280 amino acids. Three related but distinct isoforms of VDAC exist in vertebrates, but the specific roles of all the isoforms remain largely unknown.[7–9]

The basic function of VDAC is to form a diffusion pore with highly conserved characteristics in the outer mitochondrial membrane. Involvement of this/these protein(s) in metabolic pathways[10–12] and interactions with other supramolecular structures[13–17] have been claimed. The outer mitochondrial membrane functions as a link between the mitochondrial metabolism and the rest of the cell. Indeed, VDAC has been implicated in the machinery responsible for the release of pro-apoptotic factors—cytochrome c, for example—from mitochondria.[18–20] Another recent role attributed to porin/VDAC was in Ca^{2+} trafficking in the cell.[21,22]

Structural studies of VDAC have been hindered by lack of success in growing of crystals suitable for X-ray diffraction

[a] *Prof. V. De Pinto, Dr. F. Tomasello, Prof. A. Messina, Dr. F. Guarino*
Department of Chemical Sciences, Laboratory of Molecular Biology
University of Catania
Viale A. Doria, 6, 95125 Catania (Italy)
Fax: (+39) 095337036
E-mail: vdpbiofa@unict.it

[b] *Prof. R. Benz*
Department of Biotechnology Biozentrum am Hubland
University of Wurzburg
Am Hubland, 97074 (Germany)

[c] *Dr. D. La Mendola, Dr. A. Magrì, Dr. D. Milardi, Dr. G. Pappalardo*
Istituto Biostrutture e Bioimmagini, Consiglio Nazionale delle Ricerche
Viale A. Doria, 6 95125 Catania (Italy)
Fax: (+39) 095337678
E-mail: pappalardo.cnr@unict.it

studies with a sufficiently high resolution,[23] though some basic information about the pore organisation has been obtained by electron microscopy of negatively stained and frozen, hydrated two-dimensional crystals of fungal VDAC.[24] Since no atomic coordinates of VDAC are available, many efforts to design a probable model for this protein on the basis of bioinformatic analysis and experimental approaches have been made in recent years.[25–30] These models show some common features: the main secondary structures appearing in the VDACs are amphipathic β-strands, arranged to form β-barrel cylinders. This predicted feature would make VDAC very similar to bacterial porins, a family of proteins whose structures are known with atomic resolutions.[31,32] In addition, all predictions so far made for VDACs have identified the presence of a segment of α-helix, with amphipatic features, at the N termini of the proteins.

A great deal of attention has been paid to this amphipathic α-helix, because of its possible role in channel function. A succession of reports have variously proposed that the α-helix is a part of the channel walls,[25,27,29] lies transiently upon one side of the phospholipid bilayer,[26] allows some motion of the protein during the voltage-gating[33] or interacts specifically with other molecules such as cytochrome c[34] and the so-called polyanion, a potent inhibitor of porin activity.[35]

In a previous paper, we proposed a high-quality 3D model of a VDAC channel in the open conformation obtained from a threading procedure, based upon a neural network secondary structure prediction.[30] VDAC folds as a barrel formed out of 16 amphipathic β-strands with an additional amphipathic α-helix at the N terminus and exposed to the external environment. We used two neural networks designed to predict globular α-helices or membrane-embedded α-helices: it turned out that only part of the N-terminal sequence was predicted to form an α-helix, namely the sequence from residues 9 to 18.[30] This α-helix is not hydrophobic, so it is unlikely to be permanently membrane-embedded.

It is of interest to obtain structural information on this peptide fragment and to investigate its interaction with the membrane to elucidate both the conformational preferences and the functional role of this peptide region of VDAC.

In this work we have synthesised the 19-residue HVDAC1 N-terminal acetylated peptide (Ac-AVPP-TYADLGKSARDVFTK-NH_2), hereafter referred to as **Prn2–20**, encompassing the 2–20 amino acid sequence predicted to constitute the N-terminal α-helix of the VDAC protein. The secondary structure of this peptide has been investigated by CD and NMR spectroscopy under different experimental conditions, whilst DSC measurements were carried out to evaluate the affinity of the peptide for the membrane. The outcome of NMR experiments was then refined by MD calculations, allowing us to propose a reliable 3D model of the peptide in a membrane-mimicking environment. Furthermore, recombinant VDACs wholly or partially devoid of the N-terminal component were used for over-expression experiments in vivo. The results of these experiments show that the N-terminal end of porin interacts with the membrane and influences the protein activity.

Results

Circular dichroism measurements on the VDAC N-terminal peptide

The **Prn2–20** peptide corresponding to the N-terminal region of the VDAC protein was synthesised from the second amino

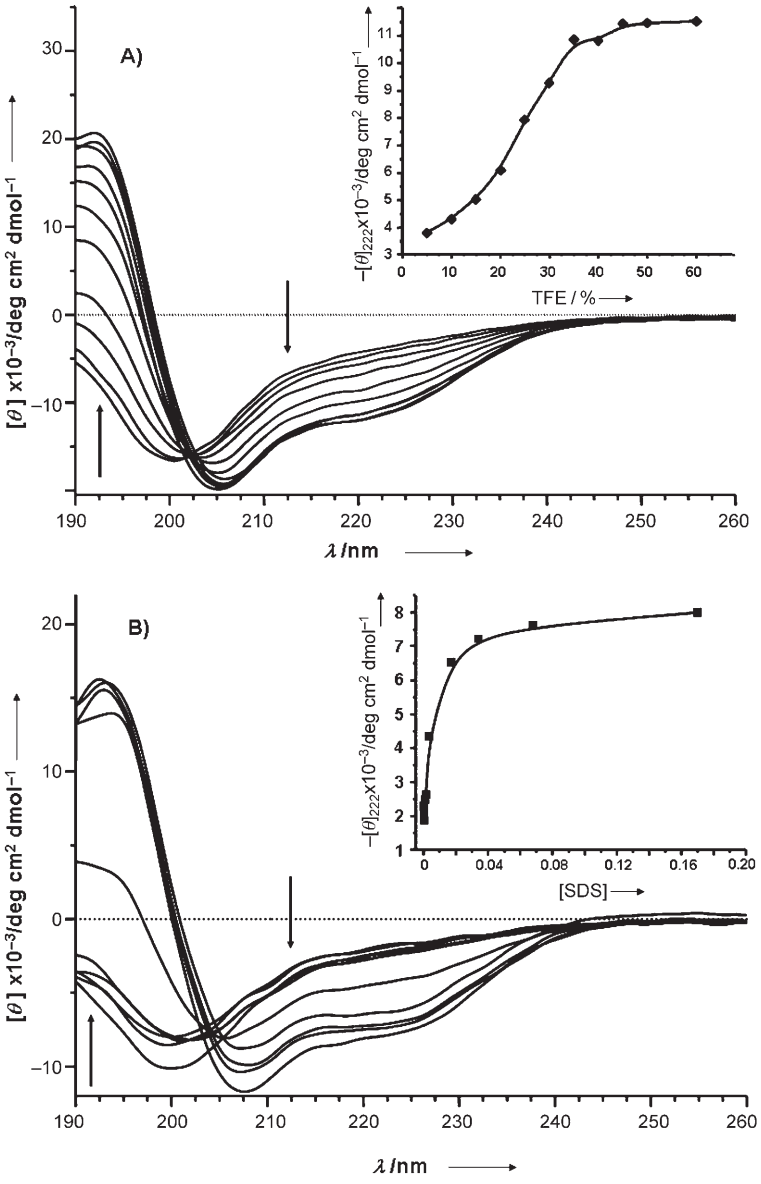

Figure 1. CD spectra of **Prn2–20** peptide recorded at: A) different percentages of TFE, and B) different SDS concentrations at pH 7.4. A) The TFE percentages used were (the pertinent CD curves are indicated by following the direction of the arrows): 5, 10, 15, 20, 25, 30, 35, 40, 45, 50 and 60%. B) The SDS concentrations used were (the pertinent CD curves are indicated by following the direction of the arrows): 1.7×10^{-4}, 3.4×10^{-4}, 8.5×10^{-4}, 1.7×10^{-3}, 3.4×10^{-3}, 1.7×10^{-2}, 3.4×10^{-2}, 6.8×10^{-2} and 0.17 mol dm^{-3}. Insets: plot of the change in $-[\theta]_{222}$ as a function of A) TFE, and B) SDS.

acid (alanine) coded in the mRNA. This alanine was reported to be acetylated in the mature protein sequence.[36] We thus mimicked the biochemical conditions of the functional protein. The pure **Prn2**–**20** peptide proved to be highly water-soluble and its CD spectra recorded in this medium, at different pH values (4–11), invariably revealed largely unstructured peptide conformations showing intense negative dichroism around 200 nm (not shown).[37] The secondary structure preferences of **Prn2**–**20** were also analysed by CD in two membrane mimetic environments: water/TFE systems and SDS micelles (Figure 1). Addition of increasing amounts of the helix-inducing solvent TFE resulted in modifications of the CD curves that progressively became more similar to that of the helical conformation, showing double minima at 206 and 222 nm and a positive band at 192 nm (Figure 1 A).[38] An isodichroic point near 203 nm is indicative of a simple mixed helix–coil equilibrium.[38,39] The mean residue ellipticity at 222 nm ($[\theta]_{222}$) depends on TFE percentage with a sigmoid profile, thus suggesting that the induction of helical structure by TFE is a cooperative process.[40] The intensity of $[\theta]_{222}$ increased up to about 40% of TFE and no further enhancement was observed at higher TFE concentrations. Measurement of $[\theta]_{222}$ is the most commonly used parameter to estimate the fraction of α-helix. At 50% TFE an average helical fraction of 0.38 was calculated by this approach (see the Experimental Section).

Behaviour similar to that seen in TFE/water mixtures was also observed in the CD spectra collected at different SDS concentration (Figure 1 B), with the peptide showing a random coil conformation in dilute SDS solution. As the SDS concentration approached its critical micelle concentration (CMC), however, the spectral profile abruptly transformed into that of the helical structure. Such an effect can also be observed by plotting the $[\theta]_{222}$ values as a function of SDS concentration (see Figure 1 B, inset). In general, α-helical profiles with lower magnitudes than in TFE/water were obtained in SDS micelles and the α-helix fraction was estimated to be around 0.28. The absence of an isodichroic point, however, might reflect the presence of other intermediate conformers that could make the equilibrium not easily interpretable in terms of simple random coil/α-helix transition.

Concentration-dependent CD studies were carried out at 25 °C and pH 7.4 in 50% TFE (2.0×10^{-6}–3.1×10^{-4} mol dm^{-3}) or 5% SDS (7.8×10^{-6}–1.25×10^{-4} mol dm^{-3}). Over the investigated concentration ranges the mean residue ellipticity $[\theta]_{222}$ is independent of peptide concentration, thus suggesting the absence of any helix–helix interaction (data not shown).

Changes in pH affected the helix structure only weakly, as evidenced by the CD spectra recorded in the pH range of 4–11 both in 50% aqueous TFE and in 5% SDS (Figure 2). Only the CD spectrum recorded at pH 11 at 50% aqueous TFE (which was acquired only partially, because of high noise below 210 nm) showed a decrease in the ellipticity at 222 nm. This suggests a probable involvement of the lysine side chain in helix stabilisation. In fact, it can be hypothesised that the deprotonation of the ε-amino groups of Lys11 and Lys19 could result in the disruption of the charge–charge interactions occurring between the carboxylate side chains of the aspartic acid residues located at positions 8 and 15, respectively. This phenomenon probably abolishes the helix-stabilizing effect generated by these salt bridges.[40]

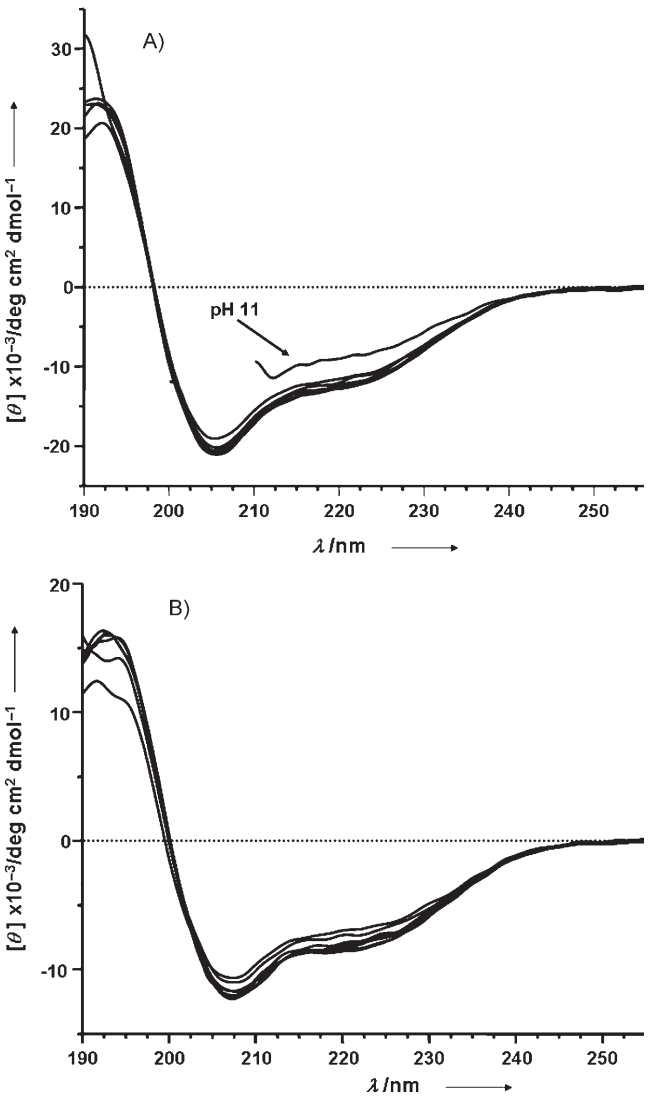

Figure 2. CD spectra of **Prn2**–**20** recorded at different pH values in: A) 50% TFE/water, and B) in 0.17 mol dm^{-3} SDS solution.

The thermal stability of the α-helix conformation was also examined by CD experiments performed as a function of temperature either in 50% TFE or 5% SDS (Figure 3). In both cases the helical content decreases with increasing temperature. A well defined non-zero isodichroic point around 202 nm is again consistent with the α-helix/coil equilibrium. The fact that there is no sharp transition during a temperature ramp (see inset in Figure 3) suggests that we have a temperature-dependent equilibrium between the two states, rather than a typical thermally induced α-helix/coil transition. Similar thermal behaviour with use of the CD technique has been reported for other peptides.[41,42]

To examine the influence of negatively charged micelles on the conformational preferences of **Prn2**–**20**, all the CD spectra carried out in SDS were also repeated in the presence of neu-

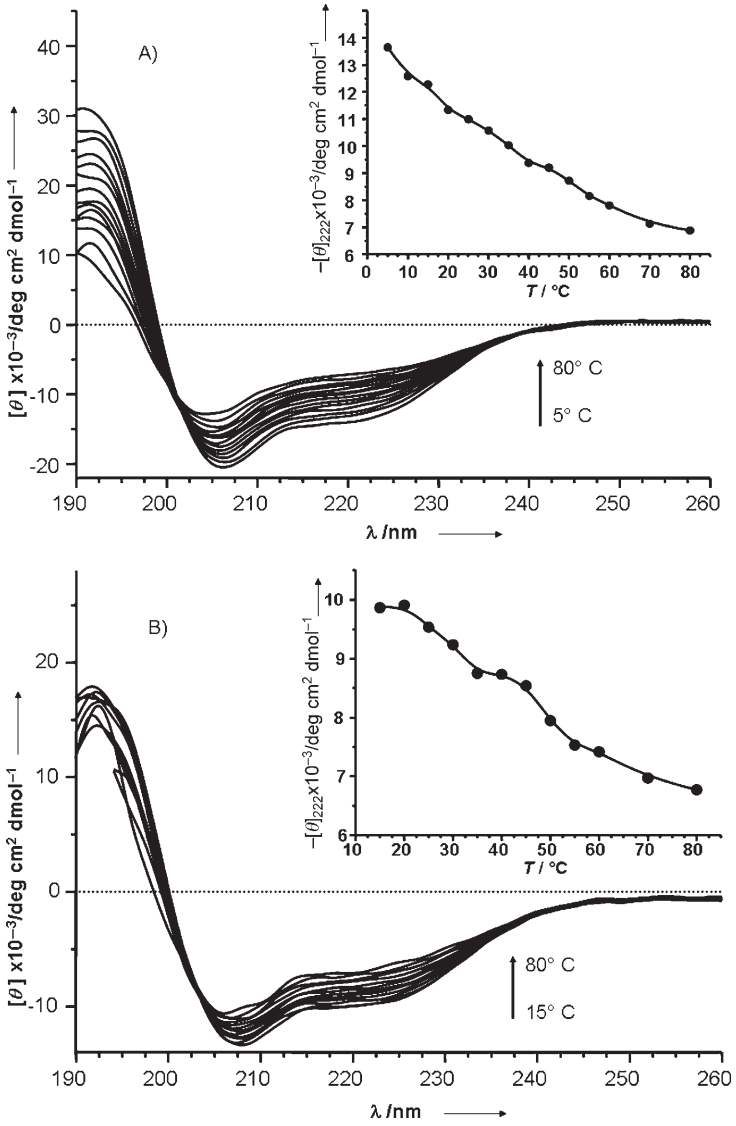

Figure 3. CD spectra of **Prn2–20** at different temperatures. CD spectra of **Prn2–20** recorded at different temperatures in: A) 50% TFE/water, pH 7.4, and B) in 0.17 mol dm^{-3} SDS, pH 7.4. Insets: plot of the change in $-[\theta]_{222}$ as a function of temperature in: A) 50% TFE/water, and in B) 0.17 mol dm^{-3} SDS solution.

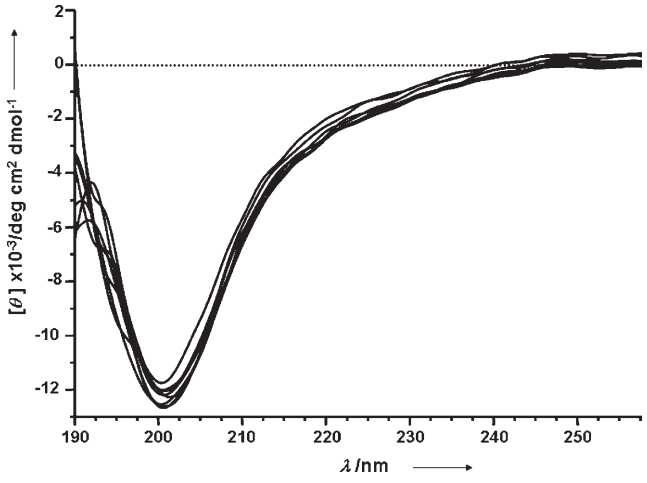

Figure 4. CD spectra of **Prn2–20** recorded at different pH values in 9.8×10^{-2} mol dm^{-3} DβM.

tral DβM (dodecyl-β-maltoside) micelles (Figure 4). None of the conformational changes observed in SDS was reproduced in DβM, in which the CD curves remained characteristic of an unstructured peptide. This different conformational behaviour is ascribable to the presence of negative charges on the surfaces of the SDS micelles, thus suggesting that electrostatic charges might play a major role in controlling **Prn2–20** interaction with micelles and its consequent folding.

Fluorescence measurements

Tyr fluorescence spectra of **Prn2–20** were measured in the presence of increasing amounts of either SDS or DβM detergents; Figure 5 shows a plot of the emission at 305 nm as a function of the detergent concentration. It is apparent that fluorescence emission is significantly enhanced as the SDS concentration increases. In contrast, addition of DβM does not noticeably modify the intensity of fluorescence emission, thus suggesting a selective interaction of **Prn2–20** with SDS micelles.

NMR analysis

NMR experiments were performed in order to localise the α-helical region within the primary sequence of **Prn2–20**. The NMR analysis was carried out both in water and in 0.17 mol dm^{-3} aqueous (5% *w/v*) SDS to make allowance for the conformational changes induced by the membrane-mimicking environment generated by SDS. The sequence-specific ^{1}H NMR assignments in both solvent systems were accomplished by DQF-COSY, TOCSY and NOESY experiments by standard procedures[43] and are reported in Table 1.

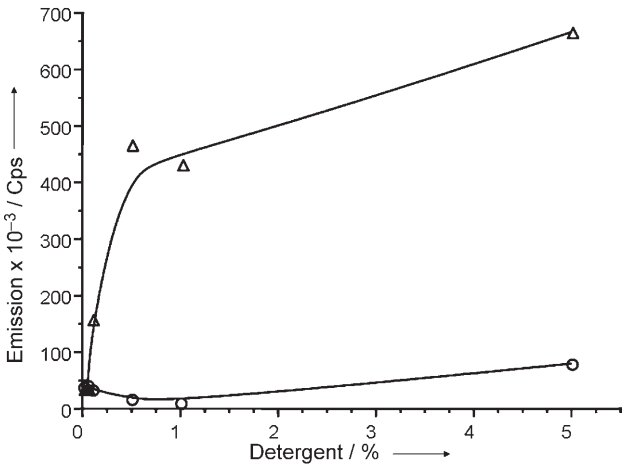

Figure 5. Tyrosine fluorescence intensity at 25 °C as a function of SDS (△) or DβM (○) detergents in aqueous solution at pH 7.0. The excitation and emission wavelengths were 275 nm and 305 nm, respectively.

Table 1. Proton chemical shifts for the peptide **Prn2–20** in H_2O, pH 5.0 (A) and in 0.17 mol dm^{-3} SDS_{-d25}, pH 5.0 (B) at 27 °C.

Res.	NH	α	β	others
A				
Ac.		2.01		
A1	8.21	4.30	1.34	–
V2	8.13	4.42	2.03	γ/γ′ 0.96/0.92
P3	–	4.70	2.37/ 1.86	γ/γ′ 2.05/2.00; δ/δ′ 3.66/3.91
P4	–	4.46	2.25/ 1.77	γ/γ′ 2.04/2.00; δ/δ′ 3.68/3.82
T5	8.07	4.25	4.16	1.19
Y6	8.14	4.55	3.08/ 2.96	(H-2,6) 7.12; (H-3,5) 6.82
A7	8.12	4.26	1.34	–
D8	8.22	4.60	2.66	–
L9	8.19	4.26	1.64	γ 1.65; δ/δ′ 0.92/0.87
G10	8.47	3.91	–	–
K11	8.01	4.32	1.86/ 1.77	γ/γ′ 1.44; δ/δ′ 1.67; ε/ε′ 3.00; $^{+}NH_3$ 7.53
S21	8.32	4.44	3.90	–
A13	8.26	4.30	1.41	–
R14	8.16	4.27	1.86/ 1.77	γ/γ′ 1.66; δ/δ′ 3.19; NHε 7.19; CNH 6.67
D15	8.15	4.57	2.77/ 2.66	–
V16	7.85	4.03	2.01	γ/γ′ 0.79
F17	8.24	4.70	3.19/ 3.06	(H-2,6) 7.28; (H-3,5) 7.35; (H-4) 7.31
T18	8.01	4.27	4.19	1.15
K19	8.18	4.26	1.86/ 1.77	γ/γ′ 1.44; δ/δ′ 1.67; ε/ε′ 3.00; $^{+}NH_3$ 7.53
NH_2				7.53; 7.12
B				
Ac.		2.01		
A1	7.86	4.35	1.32	–
V2	7.93	4.36	2.05	γ/γ′ 0.92
P3	–	4.70	2.43/ 1.92	γ/γ′ 2.06; δ/δ′ 4.00/3.58
P4	–	4.46	2.33/ 1.90	γ/γ′ 2.04; δ/δ′ 3.86/3.70
T5	7.93	4.22	4.13	1.12
Y6	7.80	4.44	3.10/ 2.94	(H-2,6) 7.05; (H-3,5) 6.81
A7	7.79	4.10	1.40	–
D8	8.06	4.53	2.76	–
L9	7.88	4.20	1.92/ 1.62	γ 1.80; δ/δ′ 0.92
G10	8.44	3.86/ 3.77	–	–
K11	7.89	4.11	1.90	γ/γ′ 1.50; δ/δ′ 1.71; ε/ε′ 3.01; $^{+}NH_3$ 7.45
S12	8.13	4.39	4.07/ 3.93	–
A13	8.35	4.06	1.50	–
R14	8.12	4.03	2.04/ 1.90	γ/γ′1.80/1.71; δ/δ′ 3.21; NHε 7.20; CNH 6.70
D15	8.03	4.49	2.85/ 2.72	–
V16	7.73	3.81	2.05	γ/γ′ 0.92/0.70
F17	7.80	4.52	3.29/ 3.02	(H-2,6) 7.31; (H-3,5) 7.24; (H-4) 7.16
T18	8.05	4.30	4.30	1.34
K19	7.85	4.20	1.89	γ/γ′ 1.50; δ/δ′ 1.71; ε/ε′ 3.01; $^{+}NH_3$ 7.45
NH_2				7.34; 7.06

In aqueous environment at pH 5 the 1D ^{1}H NMR spectrum of the peptide exhibits narrow, well resolved resonances consistent with a monomeric polypeptide chain.[44,45] Some measured $^3J_{H\alpha,NH}$ values were greater than 6.5 Hz, which is typical of conformational averaging.[43] Accordingly, the 2D NMR spectra collected under these conditions did not show any interresidue interactions that could indicate the preferred secondary structure of the polypeptide chain. The intense sequential $d_{\alpha N}$ connectivities were fairly consistent with an unstructured peptide backbone,[43] in agreement with the conclusions from CD.

The 1D proton NMR spectrum acquired in the presence of SDS micelles at pH 5 showed upfield shifts of several resonances, with concomitant line broadening of many signals. The observed trend with respect to water is indicative of structural changes induced by SDS.

Deviations of H_α chemical-shift values from those relative to random coil ($\Delta\delta H_\alpha = \delta_{observed} - \delta_{random\,coil}$) are widely used to analyse peptide secondary structure preferences. Residues in the α-helix conformation are thus readily identified from the upfield shifts of their H_α resonances, which in turn result in negative variation of the secondary chemical shifts ($\Delta\delta H_\alpha$).[46] Figure 6A compares the $\Delta\delta H_\alpha$ values calculated both in water and in SDS. Greater negative deviations are observed in SDS micelles, consistently with the presence of helix structure.[43] The NOE connectivities found in the NOESY spectra acquired in SDS medium further support the presence of helical structure. As summarised in Figure 6B, an almost complete pattern of strong sequential $d_{NN(i,i+1)}$ and weaker $d_{\alpha N(i,i+1)}$ NOE contacts was observed, together with evident $d_{\alpha N(i,i+3)}$ and $d_{\alpha\beta(i,i+3)}$ medium-range connectivities. These NOE cross peaks clearly indicate that, consistently with the CD results, **Prn2–20** can fold into a predominantly α-helical structure when bound to the SDS detergent.

Taken together, the chemical-shift values and the NOE connectivities support the presence of a helical segment spanning residues T5–V16. The N terminus seems not to be involved in the helical structure, which is due to the presence of two proline residues. Furthermore, in this region *cis*/*trans* isomerism around the V2/P3 and P3/P4 peptide bonds would be expected. The P3 residue was only observed in a *trans* conformation, as deduced from the strong cross peak between Hα of V2 and Hδ of P3. Unfortunately we were not able to infer the configuration at the P3/P4 peptide bond, because the CHα of the P3 residue resonated very close to the water presaturation frequency. However, the chemical-shift values observed for this residue both in water and in SDS agree well with those reported for a Pro residue in the *trans* conformation.[46] In any case, additional weak NMR signals accompanying residues such as Tyr and Val were noticed in the NMR spectra as well as the major ones. These small resonances were attributed to the alternative *cis* conformation at the X-Pro bond, but it was impossible to trace them along the entire peptide sequence.

From the CH_α secondary shift values and NOE connectivities collected in the presence of SDS micelles, a right handed α-helix was used as the starting structure for the reconstruction of a plausible three-dimensional model reproducing **Prn2–20**'s preferred conformation. Figure 7 shows only 20 superimposed structures, each sampled every 1000 fs of the entire MD trajec-

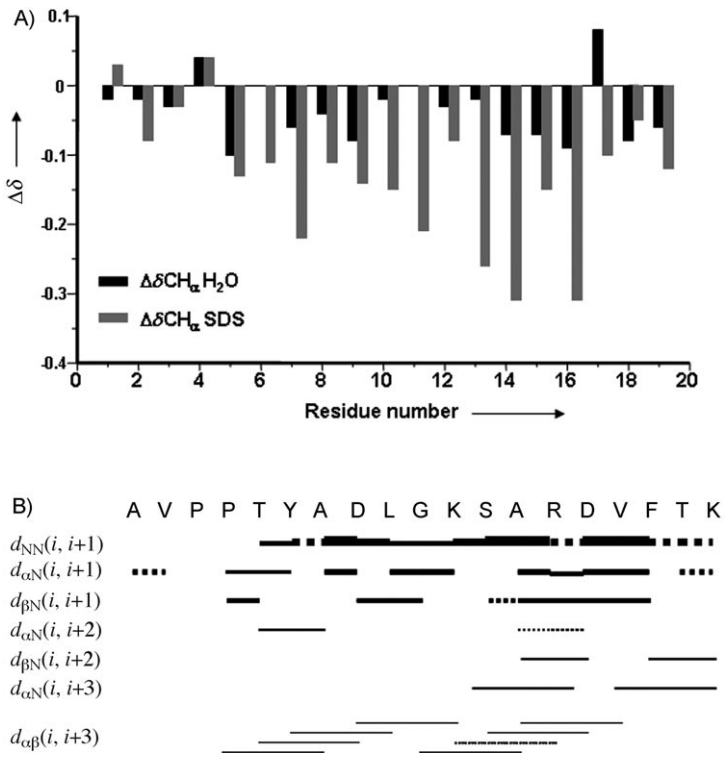

Figure 6. Chemical shift and NOE connectivities of **Prn2–20** in SDS micelles. A) Comparison of CH_α chemical shift deviation from random coil values ($\Delta\delta H_\alpha$) calculated in water or in 5% SDS, pH 5. $\Delta\delta H_\alpha = \delta_{obs} - \delta_{random\ coil}$; the random coil values were taken from ref. [46]. B) Sequential and medium-range NOE connectivities observed in 5% aqueous SDS at 27 °C and pH 5.0. The thickness of the lines reflects the relative intensities of the NOEs. ——: unambiguous NOEs, -----: possible NOEs in which chemical-shift degeneracy interferes with identification.

tory. Apart from some dynamic fraying at the termini, **Prn2–20** adopts a helical conformation over the length of the sequence from residues 5–16.

Differential scanning calorimetry of the VDAC peptide in artificial membranes

Analysis of the heat capacity changes upon the main thermal transition of a lipid/peptide system can help to clarify not only the effects of the presence of the peptide on the physical state of the membrane, but also the topological arrangement of the peptide when it is inserted into the lipid matrix.[47] In fact, the enthalpy change observed during lipid main transition can mostly be ascribed to the extent of the interaction between guest molecules and hydrophobic tails of lipids.[48] Moreover, it has been shown that T_m increases with the rigidity of the membrane, due to an interfacial lipid/peptide interaction.[48,49] With this in mind, DSC experiments were performed on both zwitterionic (DPPC; 1,2-dipalmitoyl-sn-glycero-3-phosphatidylcholine) and negatively charged (DPPS; 1,2-dipalmitoyl-*sn*-glycero-3-phosphoserine) lipid bilayers. These experiments were expected to establish: 1) whether the electrostatic properties of the membrane surface could affect the lipid/peptide interaction, and 2) whether the peptide is able either to insert itself deeply into the hydrocarbon matrix of the lipid bilayer or, alternatively, to lie on the membrane surface. Figure 8A shows DSC curves relative to the heating of DPPC/VDAC MLV (multilamellar vesicle) systems, prepared according to Method A described in the Experimental Section, and comparisons with the thermal behaviour of the pure DPPC membrane. In this case the interaction of the VDAC peptide with the bilayer is negligible. Conversely, when DPPS lipid vesicles are used as host membranes, the thermally induced transition of the lipid bilayer is affected by the presence of the VDAC peptide. In particular, when the peptide is inserted into the membrane, the DSC peak corresponding to the thermally induced main transition of the membrane is increased and its transition temperature is decreased ($T_m = 53.7$ °C) with respect to the pure DPPS (see Figure 8B). The transition enthalpy (ΔH) increases from 69.9 to 93.2 kJ mol^{-1}. In a previous paper it was shown that an amphiphilic molecule, if dispersed into the basic matrix membrane, was able to increase the ΔH associated with the gel–liquid crystal transition and to decrease the T_m.[50] This unusual behaviour was interpreted through the hypothesis that the electrostatic forces characterizing the surface of the bilayer in-

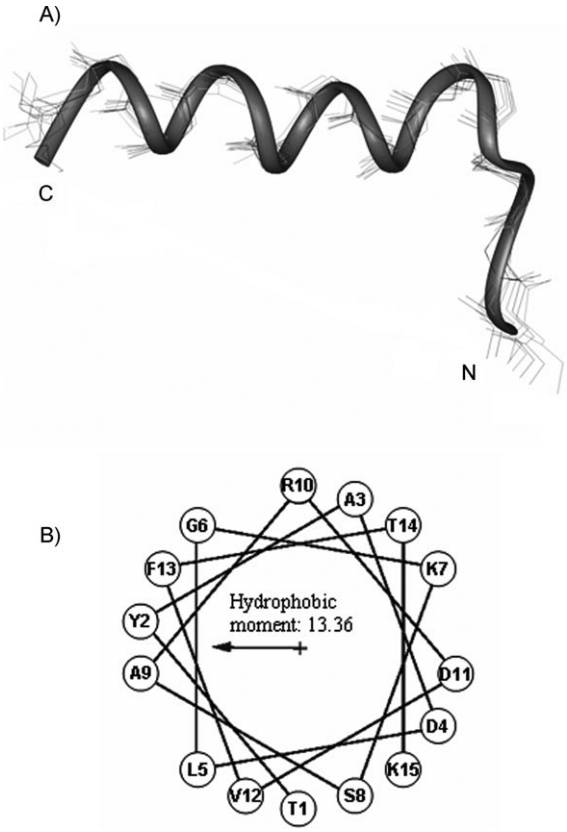

Figure 7. Structural model of **Prn2–20** derived from NMR spectra. A) Molecular dynamics-optimised structures of the possible helical conformation adopted by **Prn2–20** in SDS micelles. On the right is the N-terminal acetylated alanine. For the sake of clarity, one of the peptide backbones is presented as a ribbon. B) Helical wheel representation of the T5–K19 amino acid region of **Prn2–20** obtained with MPEx software (MPEx is available on the net at http://blanco.biomol.uci.edu/mpex).

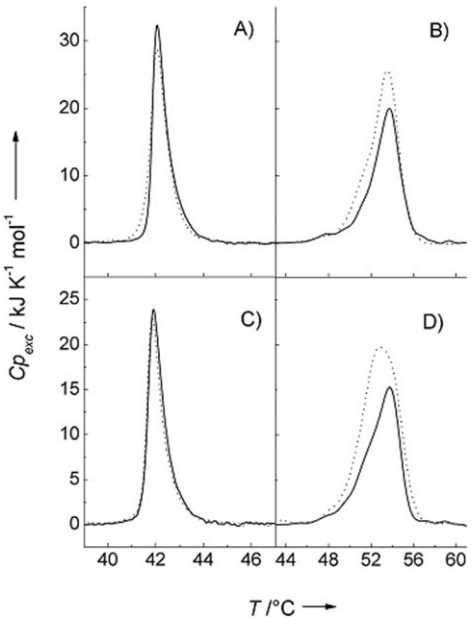

Figure 8. Thermotropic behaviour of different model membranes in the presence of **Prn2–20**. A) DSC curves of MLVs of pure DPPC (——) and DPPC/porin (····). B) DSC curves of MLVs of pure DPPS (——) and DPPS/porin (····). C) DSC curves of SUVs of pure DPPC (——) and DPPC/porin (····). D) DSC curves of SUVs of pure DPPS (——) and DPPS/porin (····). All the DSC runs were carried out as reported in the Experimental Section.

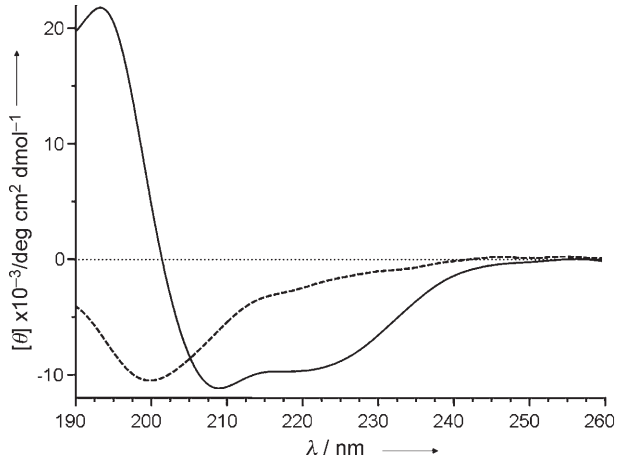

Figure 9. CD spectra of **Prn2–20** recorded in the presence of DPPC (····) or DPPS (——) membranes at 25 °C, other experimental conditions as in the DSC measurements.

volve an effective binding of the fragment with the membrane. The binding of the peptide with the membrane, in turn, increases the packing efficiency of the tail–tail contacts between the lipids. Ultimately, this increases the enthalpy of the gel-to-liquid crystal transition.

Furthermore, in order to assess whether the VDAC peptide is able to interact with the external layer of the membrane surface, a set of DSC experiments was carried out on lipid/peptide systems prepared according to Method B described in the Experimental Section. These DSC experiments were carried out on SUVs (small unilamellar vesicles) of both DPPC (Figure 8C) and DPPS (Figure 8D) and support the hypothesis that the lipid–peptide interaction occurs only when negatively charged membranes are used, and that it is mainly localised on the membrane surface.

Consistently with this hypothesis, CD spectra of **Prn2–20** collected in the presence of zwitterionic DPPC membranes (see Figure 9) revealed a random coil structure. In contrast, an α-helical structure was observed in the presence of negatively charged DPPS membranes.

N-terminal deletions abolish the pro-apoptotic effect of HVDAC1 over-expression but do not change the mitochondrial targeting of the protein

To establish the function of the mitochondrial porin N-terminal peptide in a cellular environment, we designed and expressed two recombinant proteins corresponding to the sequence of human VDAC1 but with deletion of amino acids 1–7 (Δ(1–7)HVDAC1) or amino acids 1–19 (Δ(1-19)HVDAC1). Each recombinant protein carried an HA tag at the C-end. The recombinant human VDAC1 and the two forms carrying deletions of the N-terminal end were transfected in Cos-7 cells.

It has been reported that over-expression of VDAC1 in cultured cells might imbalance the apoptotic machinery and cause the death of the cells.[51] In cells over-expressing HVDAC1, or GFP as a control, we found that only the cells transfected with HVDAC1 showed a decreased inner mitochondrial membrane potential relative to the controls (Figure 10A).

In a second experiment we evaluated the influence of N-terminal deletions upon the number of cells carrying alterations in mitochondrial ΔΨ. In this experiment (Figure 10B), the ratio

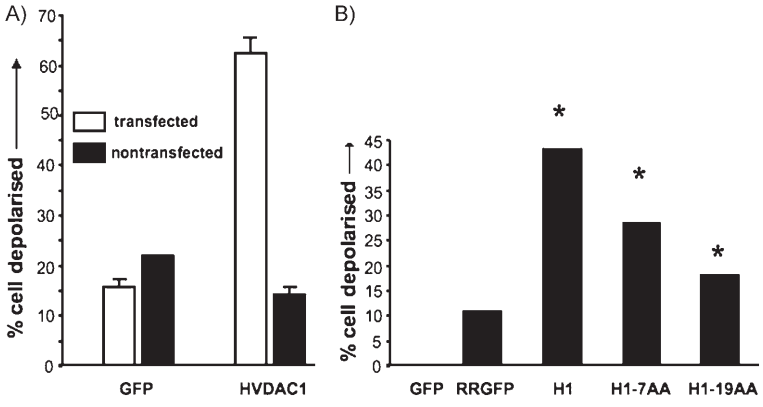

Figure 10. Determination of inner mitochondrial membrane depolarisation by flow cytometry upon over-expression of HVDAC1, Δ(1–7)HVDAC1 and Δ(1–19)HVDAC1. A) Cos-7 cells were transfected with pCMSGFP-HVDAC1-HA and pCMSGFP. After 50 h, cells were stained with TMRM and fluorescence was measured by flow cytometry. The fraction of cells in which ΔΨ was reduced or abolished was determined as percentage of TMRM negative cells among all GFP-positive ones, with use of pCMS-GFP transfected cells expressing GFP as a control. B) Cos-7 cells were transfected with pCMSGFP (GFP), pCMSRRGFP (a GFP with a targeting sequence specific for the MOM) (RRGFP), pCMSGFP-HVDAC1-HA (H1), pCMSGFP-Δ(1–7)HVDAC1-HA (H1-7AA) or pCMSGFP-Δ(1–19)HVDAC1-HA (H1–19AA). Data are shown as the mean ± SD for five independent experiments. Asterisks indicates a significant difference in relation to the pCMS-GFP transfected cells group ($p < 0.001$, χ^2 test).

of the depolarised cells was normalised with respect to the number of transfected cells. The over-expression of HVDAC1 causes depolarisation of mitochondrial $\Delta\Psi$. When the cells were transfected with mutant HVDAC1 with deletions at the N-terminal end we found a progressive decrease in the number of depolarised cells normalised to the transfected cells. As a control the transfection with RRGFP, targeted specifically to the MOM,[52] or with the GFP alone, showed a little or no influence upon the number of cells with depolarised mitochondria. This result suggests an involvement of the N-terminal end of VDAC1 in the apoptotic events leading to the inner mitochondrial membrane depolarisation.

We also wanted to establish whether the two mutant proteins (Δ(1–7)HVDAC1) and (Δ(1–19)HVDAC1) were correctly targeted to mitochondria. The recombinant human VDAC1 and the two forms carrying N-terminal end deletions were transfected in Cos-7 cells. Confocal microscope imaging revealed HA staining (specific for HVDAC1), cytochrome c, and their merging (Figure 11). There is a clear overlapping of the red (HVDAC1 staining) and green (cytochrome c), as shown in the merging of the virtual colours. This was true not only for the VDAC1 but also for both the mutants carrying deletions at the N-terminal end, demonstrating that such deletions do not change the mitochondrial targeting of this protein.

Discussion

The N-terminal peptide of human VDAC1 is unstructured in water but can switch to an α-helix in a hydrophobic and charged environment

In a recent work we put forward a high-quality 3D model of a VDAC channel in the open conformation obtained from a threading procedure based upon a neural network secondary

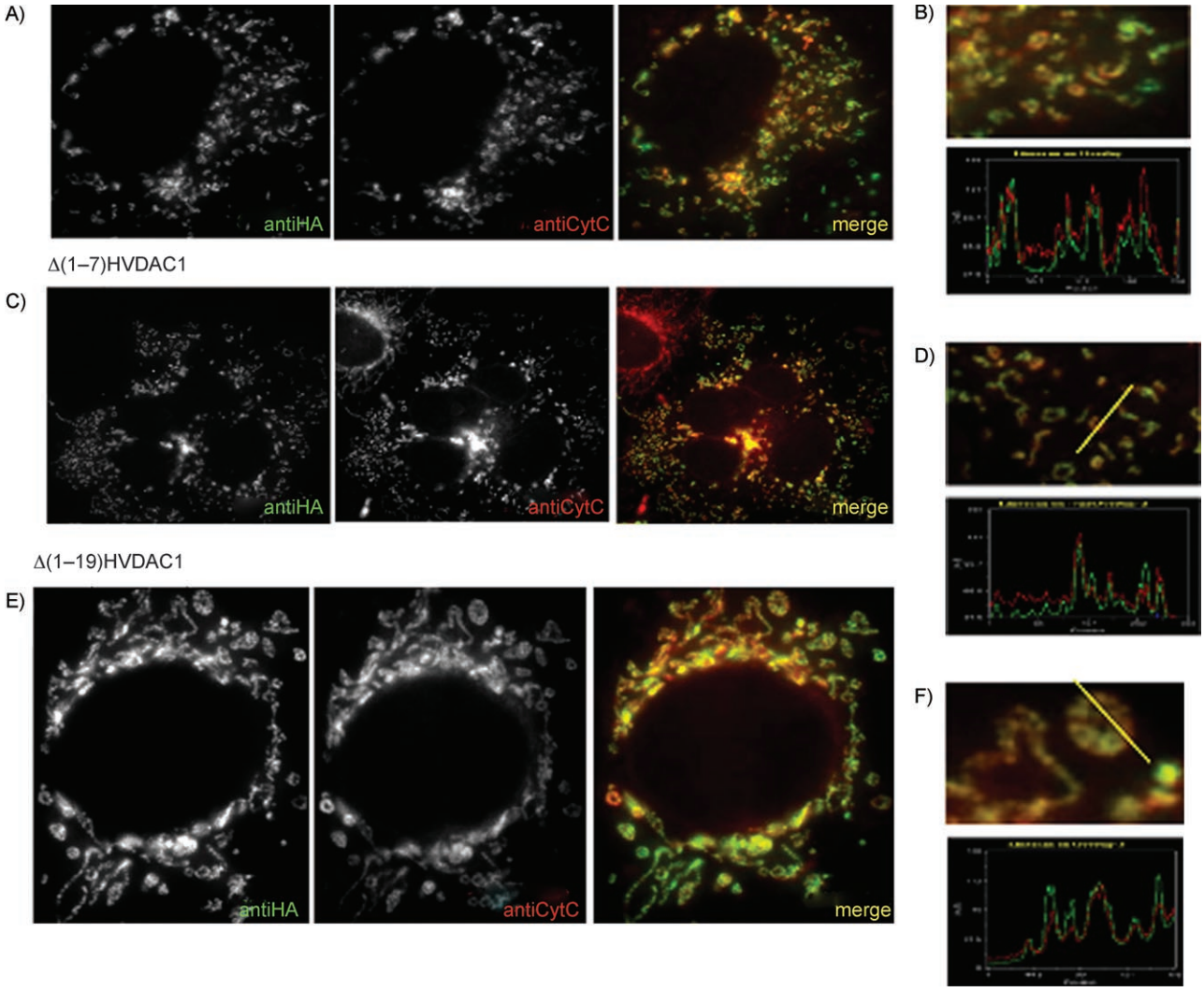

Figure 11. Subcellular localisation of transfected HVDAC1, Δ(1–7)HVDAC1 and Δ(1–19)HVDAC1. Cos-7 cells were transfected with: A) pCMSGFP-HVDAC1-HA, C) pCMSGFP- Δ(1–7)HVDAC1-HA and E) pCMSGFP- Δ(1–19)HVDAC1-HA. The fixed cells were stained either with an anti-HA antibody, revealed by a FITC-conjugated secondary antibody, or with an anti-cytochrome c, an endogenous mitochondrial protein, revealed by a TRITC-conjugated secondary antibody. Fine analysis of the fluorescence distribution (merge, right panel) reveals a substantial colocalisation of HVDAC1 and cytochrome c. Panels B, D and F show line scanning of mitochondria enlargement with the distribution of fluorescence profiles for: B) HVDAC1, D) Δ(1-7)HVDAC1 and F) Δ(1-19)HVDAC1. Similar fluorescence distributions and similar merge profiles were obtained with both N-terminal end mutants.

structure prediction.[30] In this model, VDAC was predicted to fold as a barrel formed out of 16 amphipathic β-strands with an additional amphipathic α-helix at the N terminus, protruding outside or interacting with the membrane surface. This N-terminal α-helix extended from residue 9 to residue 18, whilst residues 1–8 were predicted to exist in a more random conformation. Interestingly, these same properties were found in VDAC proteins as evolutionarily distant as mammals and fungi.[30]

The detailed spectroscopic study reported here represents the first direct analysis of the conformational features shown by **Prn2–20**, a peptide fragment corresponding to the 2–20 amino acid sequence found in the N-terminal region of the human VDAC isoform 1. The CD spectroscopy suggests that **Prn2–20** possesses a good propensity to fold into an α-helix conformation in a hydrophobic environment, although it remains unstructured in aqueous solution. The estimated helical content was greater in the presence of TFE than in SDS, consistently with previous CD studies carried out on similar peptide derivatives from the N terminus of the VDAC of *N. crassa*.[53] The fact that non-ionic dodecyl β-maltoside micelles were ineffective in promoting the α-helix conformation of **Prn2–20** underlines the distinctive role played by electrostatic charges in the conformational transition. Moreover, on the basis of the CD results obtained at different SDS concentrations, it can be concluded that **Prn2–20** does not tend to assume a β-sheet conformation, because it is known that SDS should promote β-sheet structures in peptides with an inherent propensity to this at concentrations below the CMC.[54]

Since SDS might be a better model than TFE with which to mimic the membrane environment, the helical structure of **Prn2–20** was studied in this medium. The helical region does not span the whole peptide sequence, being mainly between residues T5–V16, with some flexibility at the C-terminus. Such a result is in good agreement with those of Casadio et al.[30] The helical wheel projection of the T5–K19 segment shows that hydrophobic residues cluster on one face of the helix, whereas charged and polar residues are segregated on the opposite side (Figure 7B). This suggests that the helix structure could be stabilised either by hydrophobic and/or by charge–charge interactions. Because of the different behaviour of **Prn2–20** in SDS and DβM micelles, it is apparent that electrostatic interactions are fundamental in stabilizing helical structure, at least in a micellar environment.

Interaction of the HVDAC1 N-terminus with membranes

The amphipathic nature of the N-terminal helix of human VDAC protein might correlate with a relevant functional role, so it becomes important to obtain more details about the topology of **Prn2–20** in lipid membranes. With this as a goal, DSC experiments were carried out on **Prn2–20**/membrane systems. The outcome of these DSC experiments was expected to provide hints either on the capability of this peptide to interact with lipid membranes or on its location in the bilayer. Unlike in the case of DPPS vesicles, the addition of **Prn2–20** to DPPC SUVs or MLVs did not modify the thermotropic behaviour of the bilayer. Phosphatidylserine has a negative charge in excess over phosphatidylcholine, which is zwitterionic. Our results in this model system thus suggest that the presence of the hydrophobic environment alone is not enough to enable the N-terminal peptide to interact with membranes and that the presence of negative charge(s), which in turn promote(s) the interaction of **Prn2–20** with the external surface of the membrane, is required. In the cell, this specific environment might be provided by the surrounding part of the proteic pore or by the phospholipid bilayer. Alternatively, the N-terminal peptide might stay in the hydrophilic milieu as an unstructured peptide, making it an accessible target not only to specific antibodies, as demonstrated,[26,35,55] but also to modifying enzymes or other extramembranous structures.[34,35] Its putative mobility contrasts nicely with the rigidity of the β-barrel walls and could be the reason for the well known difficulty in obtaining ordered crystals of VDACs.

Is the N-terminal sequence part of the voltage sensor?

Results obtained in reconstitution experiments indicate that the N-terminal portion of VDAC is essential for proper functioning of the pore. According to Colombini et al.,[56] the N-terminal α-helix and the nearby β-strand are the voltage sensor of the pore: that is, the molecular structure responsible for sensing voltage variations across the membrane. Raising the voltage across a membrane containing a reconstituted VDAC1 pore does indeed have the consequence of reducing the current flowing through the pore. Deletion mutants at the N-terminal end have been produced for the *N. crassa* (nc) and the *Saccharomyces cerevisiae* (sc) VDACs,[53,57] ncVDAC ΔN(2–12)[58] and scVDAC ΔN(1–8)[59] and showed loss of voltage dependence and instability of the open state of the channel. The deletion of further sequence at the N-terminal end[58] enhances the alterations in single-channel activity, strengthening the idea that this protein domain is highly important for the pore-formation.

From evaluation of reconstitution experiments, Koppel et al. concluded that the N-terminal deletions support those structural models that have the N-terminal domain forming an integral part of the channel wall in VDAC's open state.[29,59] From similar data, Popp et al. speculated that the N-terminal end might play a role in the stabilisation of the open pore.[58]

Is the N-terminal sequence part of the pore wall?

The NMR reconstruction of the sequence structure confirmed our earlier prediction that the amphipathic α-helix spans only a segment of it.[30] The preceding amino acids form a diproline hook-like structure that is quite stable, but cannot be involved in the α-helix.

We believe that it is unlikely that the N-terminal domain can form part of the channel wall since it is partially unstructured and because 11 amino acids cannot form an α-helix long enough to span the membrane, even with consideration of the tilt of the pore.[34,60]

The N-terminal sequence is one of the most immunogenic parts of the VDAC.[26,34,55] Monoclonal antibodies against this peptide have been produced, and these antibodies invariably detected this moiety outside the membrane.[34,55] In a study reporting the interaction of Fab fragments derived from antibodies specific for residues 1–20 of *N. crassa* VDAC with 2D crystals of the channel, it was found that the immunochemical binding was at a corner of the unit cell, extending laterally out from the lumen.[53] The authors suggested that the results obtained were consistent with the α-helical structure projecting laterally away from the pore. This "flap" was depicted in a 3D reconstruction of the pore resulting from gold-glucose embedding,[33] and it was proposed that it could correspond to the loop 3 domain of bacterial porins, a large domain that extends inside the pore.[33] In the same reconstruction this "flap-like region" occurs close to an area of absence of mass (groove): Mannella's conclusion is that this structural information makes it probable that the N-terminal region might be a mobile component of the pore, involved in the process of gating.[33] According to this work, the N-terminal end would be able to move on the cytoplasmic side of the mitochondrial porin. Although not a truly structural part of the pore, it could be able to reinforce the walls of the channel by bending inside the pore and pushing on the wall. The deletion of such an important structural element could result in a strong impairment of the structure of the pore and in the collapse of the VDAC pore in a way similar to that observed with the deletion of loop 3 in bacterial porins.

The N-terminal sequence is not involved in the mitochondrial targeting of HVDAC1

To complement the structural information we produced recombinant proteins devoid of the same peptide and used them to transfect cells to reveal any functional consequences of the peptide deletion.

N-terminally deleted HVDAC1 mutants were found to have no influence on the insertion of the whole protein in the mitochondria. This result indicates that it is not a targeting sequence. The posttranslational import pathway of porin/VDAC has been elucidated in some detail but it is not fully understood. The most recently proposed mechanism for sorting of mitochondrial β-barrel precursors involves a TOB complex that would mediate the insertion of the precursor presented from the inner side of the outer membrane.[61] It is not clear either what mechanism is used by the mitochondrial β-barrel precursors to cross the outer membrane, neither what are and where in the candidate imported proteins are the targeting and insertion signals. Our experiments clearly demonstrate that such signal sequences are not present in the N-terminal sequences deleted here.

Deletion of the N-terminal sequence prevents apoptosis by HVDAC1 over-expression

We also measured the variability of $\Delta\Psi$, the membrane potential of the mitochondrial inner membrane, a change in which might impact on the cell life and which is regarded as a trigger for apoptosis.[51] It has been reported that over-expression of HVDAC1 in U-937 and Jurkat cells results in cell death.[51] A straightforward interpretation is that HVDAC1 over-expression might produce an increase in the leakage of the outer membrane or an alteration in the components ratio of the permeability transition pore. Another possibility, proposed by Zalk et al., is that over-expression of HVDAC1 would promote dynamic HVDAC1 oligomerisation, a process leading to the release of cytochrome c.[62] Although we did not observe any helix–helix interaction in **Prn2–20**, we cannot exclude the possibility that this might occur when this peptide is part of the whole protein.

Upon HVDAC1 over-expression the inner mitochondrial membrane became depolarised, whilst the progressive deletions of the N-terminal were able to reduce or prevent this effect. From this result it is clear that the N-terminal sequence is important for the regulation of cellular functions indispensable for the proper work of the mitochondrion and for its relationship with the machinery involved in the life/death switching of the cell.

Conclusions

We have produced the first structural evidence relating to the sequence of the channel-forming protein HVDAC1 by determining the NMR structure of its N-terminal peptide. Despite the relevance of this protein in cell physiology and apoptosis, there had previously been no information on the HVDAC1 at the atomic level. Contrary to the several bioinformatics predictions available, we found for the first time that this peptide can switch between two different structures, depending on the environment. In addition, only part of the sequence is able to form an α-helix; this affects the organisation of the pore. Functional experiments in which the same peptide was progressively deleted from the N terminus confirmed that this part of the protein is essential for the proper physiological activity of the mitochondrion. Our results underscore the distinctive structural and functional role of the N terminus of HVDAC1 and describe it at a molecular level.

Experimental Section

Chemicals: All *N*-fluorenylmethoxycarbonyl-protected (Fmoc-protected) amino acids were obtained from Novabiochem (Switzerland); the other chemicals for the peptide synthesis were from Applied Biosystems. *N*-Hydroxybenzotriazole (HOBT), triisopropylsilane (TIS), trifluoroacetic acid (TFA), ethanedithiol (EDT), sodium dodecylsulfate (SDS), dodecyl β-maltoside (DβM) and trifluoroethanol (TFE) were purchased from Sigma–Aldrich. 1,2-Dipalmitoyl-sn-glycero-3-phosphoserine (DPPS) and 1,2-dipalmitoyl-sn-glycero-3-phosphatidylcholine (DPPC) were from FLUKA. All other chemicals were of the highest available grade and were used without further purification.

Peptide synthesis and purification: Peptide Ac-AVPPTYADLGK-SARDVFTK-NH_2 (**Prn2–20**) was synthesised on a Pioneer Peptide Synthesiser. All residues were introduced by the HATU/DIEA activation method by Fmoc chemistry on Fmoc-PAL-PEG-PS resin (substi-

tution 0.25 mmol g^{-1}, 0.1 mmol scale synthesis, 0.4 g of resin). The synthesis was carried out with a fourfold excess of amino acid at every cycle and each amino acid was recirculated through the resin for 35 min. Removal of Fmoc protection during synthesis was achieved with piperidine in DMF solution (20%). N-terminal acetylation was performed by treating the fully assembled and protected peptide resin (after removal of the N-terminal Fmoc group) with a solution containing acetic anhydride (6% *v/v*) and DIEA (5% *v/v*) in DMF. The peptide was cleaved off from the resin and simultaneously deprotected by treatment with a mixture of TFA/thioanisole/phenol/H_2O/EDT/TIS (81.5:5:5:5:2.5:1 *v/v*) for 2 h at room temperature. The crude product was precipitated with cold diethyl ether and lyophilised. Peptide purification was accomplished by preparative reversed-phase HPLC by use of a Vydac C_{18} 250× 22 mm (300 Å pore size, 10–15 mm particle size) column with a water/acetonitrile gradient containing 0.1% (*v/v*) TFA. Peptide purity was checked by analytical RP-HPLC by use of a Vydac C_{18} chromatographic column (150×4.6 mm; 5 μm particle size and 300 Å pores). Sample identity was confirmed by ESI-MS (calcd for $C_{94}H_{149}N_{25}O_{28}$: 2077.36; found 1039.7 $[M+2H]^{2+}$; 693.5 $[M+3H]^{3+}$).

Circular dichroism (CD): The CD spectra were recorded at 300 K under a constant flow of nitrogen on a Jasco model J-810 spectropolarimeter that had been calibrated with an aqueous solution of (1*R*)-(−)-10-camphorsulfonic acid (ammonium salt).[63] Experimental measurements were carried out under a variety of experimental conditions including at different pH values, at different percentages of aqueous TFE or detergent (SDS or DβM) concentrations and in DPPC or DPPS membranes. Samples containing DPPC or DPPS membranes were sonicated for 45 min prior to the acquisition of CD spectra. The CD spectra were recorded in the UV region (190–260 nm) with use of a 1 mm path length cell with peptide concentrations of 1.0×10^{-5} mol dm^{-3}. The spectra each represent the average of 8–20 scans. CD intensities are expressed as mean residue ellipticity $[\theta]$ (° cm^2 $dmol^{-1}$). The fraction of helicity ($f_{\alpha H}$) for **Prn2**–**20** in an α-helical conformation was estimated from the equation $f_{\alpha H}=(\theta_{obs}-\theta_{RC})/(\theta_H-\theta_{RC})$, where θ_{obs} is the observed ellipticity and θ_{RC} and θ_H are the ellipticity values for a completely random and a completely helical peptide with a length equal to that of **Prn2**–**20**, respectively.[64] Values for θ_H (-31.8×10^3 ° cm^2 $dmol^{-1}$) and θ_{RC} (895 ° cm^2 $dmol^{-1}$) were calculated as described in the literature.[64,65] All ellipticity values were at 222 nm.

NMR spectroscopy and structure calculation: All NMR spectra were acquired at 27 °C on a Varian INOVA Unity-plus spectrometer operating at 499.884 MHz. Lyophilised samples (5×10^{-3} mol dm^{-3} concentration) were dissolved in H_2O/D_2O (90:10) or in SDS_{-d25} (0.17 mol dm^{-3}) in H_2O/D_2O (90:10). Trimethylsilylpropionic acid (TSP) was used as an internal standard. The pH of the solution was adjusted to pH 5.0 by addition of the appropriate acid or base solution. The electrode-measured pH value was uncorrected for the isotope effect. 1D spectra were generally acquired with 32 K data points over a spectral width of 6000 Hz.

2D experiments: DQF-COSY,[66] TOCSY,[67] ROESY[68] and NOESY[69] were typically acquired in the phase-sensitive mode by the States–Haberkorn method with 2048 data points in the t_2 dimension and 512 t_1 increments. Water saturation was achieved by low-power irradiation during the relaxation delay. TOCSY spectra were acquired with a spin locking field of 7 kHz at a mixing time of 80 ms. ROESY spectra were run by use of a 2 kHz spin locking field at a mixing time of 250 ms. Mixing times of 300 and 500 ms were used in the NOESY experiments. The structural information obtained from the NMR analysis was used to generate a 3D model of the VDAC peptide in silico. The initial α-helical structure was built with the aid of the BIOPOLYMER module in the InsightII software suite. The residues Val2–Pro3 and Pro3–Pro4 were fixed in a *trans* configuration as deduced from NMR data. Interproton distance restraints were generated from the 2D NOESY data and used as inputs in Discover calculations. The initial structure was first energy-minimised in order to release the side-chain strains before the simulations were begun. The energy-minimised structure was then immersed in a thermal bath at 298 K. Productive MD simulations were carried out in vacuum up to 20 ps with a time step of 1 fs by use of the program Discover[3], which adopts the native AMBER forcefield. Nonbond interactions were handled by use of a cut-off distance of 15 Å.

Fluorescence emission: Fluorescence measurements were performed on a Jobin–Yvon Fluorolog 3 spectrofluorimeter operating in photon-counting mode. The excitation wavelength was 275 nm and the emission was scanned from 285 to 350 nm. In all the experiments, the appropriate reference spectrum of the detergent water solution was subtracted from the corresponding sample spectrum in order to minimise light-scattering effects. Six independent sample solutions were prepared, in which the peptide concentration was set at 1×10^{-5} mol dm^{-3}, whilst the detergent percentages ranged from 0.01 to 5% (i.e., for SDS from 3.4×10^{-4} to 0.17 mol dm^{-3}; for DβM from 2.0×10^{-4} to 0.1 mol dm^{-3}). Data were then corrected for the inner filter effect and for the trivial absorption of the incident light by the detergent according to a procedure reported in the literature.[70]

DPPS and DPPC membranes for differential scanning calorimetry: Model membranes were prepared as described elsewhere.[71] Briefly, solutions of the pure phospholipids in $CHCl_3$ were dried under a nitrogen flow and evaporated to dryness under high vacuum in round-bottomed flasks. The resulting lipid film on the wall of the flask was hydrated with an appropriate volume of 1.0×10^{-2} mol dm^{-3} phosphate buffer and dispersed by stirring in a water bath set at 4 °C above the gel/liquid-crystal transition temperature of the membrane to produce multilamellar vesicles (MLVs). The final nominal concentration of the lipid was 2 mg mL^{-1}. Small unilamellar vesicles (SUVs) were prepared by sonication of MLVs. Typically, 1 mL volumes were sonicated for 45 min above the corresponding transition temperatures (T_ms) of the phospholipids with a 90% duty cycle. Sonicated vesicles were rapidly cooled to room temperature and used within 45 min to prevent coalescence.

Incorporation of peptide fragments into model membranes: Two different methods to prepare mixed lipid/peptide bilayers were applied. A) The peptide fragment was initially dissolved in the same organic solution ($CHCl_3$) of the phospholipid (peptide/lipid molar ratio of 1:10), and the lipid film was next hydrated and extruded/sonicated by the procedure described above. B) An appropriate amount of peptide was added to previously prepared SUVs of DPPS or DPPC to give a final peptide/lipid molar ratio of 1:10. The mixture was initially vigorously vortexed for 15 min and, unless otherwise specified, analysed immediately.

Differential scanning calorimetry (DSC): DSC scans were carried out with a second-generation high-sensitivity SETARAM micro differential scanning calorimeter (microDSC II) with 1 mL stainless steel sample cells, interfaced with a BULL 200 Micral computer. The sampling rate was 1 point s^{-1} in all measuring ranges. The buffer solution without the sample was used in the reference cell. Both the sample and reference were heated with a precision of 0.05 °C at a scanning rate of 0.5 °C min^{-1}. In order to obtain the excess heat capacity (Cp_{exc}) curves, buffer–buffer base lines were recorded at the same scanning rate and were then subtracted from sample

as previously described.[72] Calibration in energy was obtained by use of a definite power supply, electrically generated with an EJ2 SETARAM Joule calibrator, within the sample cell. To check the reproducibility of the results, three different samples were analysed. All DSC experiments were repeated after 24 and 48 h, but no kinetic effects were ever detected.

Recombinant cDNA and vectors: For transfection in eukaryotic cells, the cDNA coding for isoform 1 of human VDAC tagged at the C-end with the hemaglutinin epitope (HA) was PCR-amplified from pSEYc58 construct (kindly provided by M. Forte, Oregon) with use of an upper primer incorporating a NheI site (5′-CTA GCT AGC CAA CAA TGG CTG TGC CAC CCA-3′) and a lower primer with an MluI site (5′-CGA CGC GTT TAA GCA TAA TCT GGA ACA TC-3′). The QuickChange site-directed mutagenesis kit (Stratagene) was used to delete the N-terminal sequence. Δ(1–7)HVDAC1 was obtained by use of the upper primer Δ(1–7)HVDAC1For (5′-CTC ACT ATA GGC TAG CAT GGA TCT TGG CAA ATC TGC-3′) and the lower primer Δ(1–7)-HVDAC1Rev (5′-GCA GAT TTG CCA AGA TCC ATG CTA GCC TAT AGT G-AG-3′). Δ(1–19)HVDAC1 was obtained by use of the upper primer Δ(1–19)HVDAC1For (5′-CTC ACT ATA GGC TAG CAT GGG CTA TGG ATT-TGG CTT AAT-3′) and the lower primer Δ(1–19)HVDAC1Rev (5′-ATT-AAG CCA AAT CCA TAG CCC ATG CTA GCC TAT AGT GAG-3′). The PCR reaction was performed by the manufacturer's method with *Pfu* Turbo DNA polymerase (2.5 units) and 125 ng of primers. The amount of template used was 10 ng. The PCR product was digested by use of *Dpn*I (10 units) at 37 °C over 1 h. The digested DNA (1 μL) was transformed in competent *E. coli* M15 cells. The DNA purified from single colonies was sequenced to check the products. The PCR-amplified HVDAC1-HA cDNAs were cloned between the NheI and MluI sites of pCMS-GFP (Clontech).

Cell culture and transfection: HeLa (human cervix carcinoma), and Cos-7 cells (transformed monkey kidney fibroblast) were grown at 37 °C under an atmosphere of 95% air and 5% CO_2 in Dulbecco's MEM medium (Gibco, Invitrogen) and supplemented with 10% of fetal calf serum (FCS; Gibco, Invitrogen). Transient transfections with mammalian expression vectors were performed with 2 μg mL^{-1} DNA and cationic Exgene500 (Euromedex) by the manufacturer's method.

Determination of apoptosis-associated alterations ($\Delta\Psi$ collapse) by flow cytometry: $\Delta\Psi$ was measured with the aid of tetramethylrhodamine methyl ester (TMRM; Molecular Probes, Eugene, OR). After treatment, adherent cells were washed with PBS incubated for 30 min at 37 °C with Krebs Ringer Buffered Saline supplemented with Verapamil (Sigma, 2.0×10^{-5} mol dm^{-3}) and TMRM (2.0×10^{-7} mol dm^{-3}). Cells were then detached by short treatment with tryspin-EDTA and collected. At least 20000 cells per sample were analysed by use of a PAS Laser/UV flow cytometer (Partec). The data obtained were acquired, gated, compensated and analysed by use of FlowMax software (Partec). All data presented here were representative of at least three sets of independent experiments. The differences between different groups were examined by use of χ^2 tests. A P value below 0.001 was considered to be significant.

Indirect immunofluorescence of adherent cells and imaging analysis: After appropriate time for protein expression, cells grown on the coverslip were washed with PBS and fixed in formaldehyde (3.7%) over 20 min at room temperature. Fixed cells were permeabilised with Triton X-100 (0.5%), unspecific binding was blocked by 30 min of incubation in 0.2% gelatin in PBS, and staining was performed by use of specific primary antibodies against the HA tag (Roche), as well as a monoclonal antibodies against native cytochrome c (PharMingen). After washing, cells were incubated with the corresponding secondary antibodies conjugated with FITC (Sigma). Cells were observed with the aid of a Zeiss Axiovert 100 M inverted motorised microscope. For each acquisition channel, the results are presented as quantitative pseudocolor images and graphs constructed by performing line scan intensity measurement on each image. To quantify global variations of the signals (HA, cytochrome c, mtBFP) on whole cells, we measured their levels of spatial heterogeneity rather than their peak intensities. Indeed, the spatial heterogeneity of the signal is an indicator of the level of compartmentalisation of the probe, which in the case of cytochrome c or Bax indicated the relative amount of protein present at the level of mitochondria. Computation, for each individual cell, of the spread of pixel intensity can assess the spatial heterogeneity of the signal. This spread is defined by the standard deviation of the pixel intensity in space. Pixels measurement was also used for morphological and size investigations of mitochondria in treated cells. All data presented here were representative of at least three sets of independent experiments.

Acknowledgements

This work was supported by FIRB2003_RBNE03PX83, by the University of Catania and the CNR (Rome), as well as by the Deutsche Forschungsgemeinschaft and the Fonds der Chemischen Industrie. The authors acknowledge the assistance of F. Ichas and F. De Giorgi-Ichas in the confocal microscopy experiments. Thanks are also due to R. Lauceri for helpful assistance in fluorescence experiments.

Keywords: apoptosis · calorimetry · circular dichroism · ion channels · NMR spectroscopy

[1] M. Colombini, *J. Membr. Biol.* **1989**, *111*, 103 – 111.
[2] R. Benz, *Biochim. Biophys. Acta* **1994**, *1197*, 167 – 196.
[3] E. Blachly-Dyson, M. Forte, *IUBMB Life* **2001**, *52*, 113 – 118.
[4] V. Shoshan-Barmatz, D. Gincel, *Cell Biochem. Biophys.* **2003**, *39*, 279 – 292.
[5] C. A. Mannella, W. D. Bonner Jr, *Biochim. Biophys. Acta* **1975**, *413*, 213 – 225.
[6] V. De Pinto, O. Ludwig, J. Krause, R. Benz, F. Palmieri, *Biochim. Biophys. Acta* **1987**, *894*, 109 – 119.
[7] M. J. Sampson, R. S. Lovell, W. J. Craigen, *J. Biol. Chem.* **1997**, *272*, 18966 – 18973.
[8] A. Messina, M. Oliva, C. Rosato, M. Huizing, W. Ruitenbeek, L. P. van den Heuvel, M. Forte, M. Rocchi, V. De Pinto, *Biochem. Biophys. Res. Commun.* **1999**, *255*, 707 – 710.
[9] Z. Rahmani, C. Maunoury, A. Siddiqui, *Eur. J. Hum. Genet.* **1998**, *6*, 337 – 340.
[10] D. Ardail, J. P. Privat, M. Egret-Charlier, C. Levrat, F. Lerme, P. Louisot, *J. Biol. Chem.* **1990**, *265*, 18797 – 18802.
[11] J. E. Wilson, *J. Exp. Biol.* **2003**, *206*, 2049 – 2057.
[12] J. G. Pastorino, J. B. Hoek, *Curr. Med. Chem.* **2003**, *10*, 1535 – 1551.
[13] V. Adams, L. Griffin, J. Towbin, B. Gelb, K. Worley, E. R. B. McCabe, *Biochem. Med. Metab. Biol.* **1991**, *45*, 271 – 291.
[14] V. Le Mallay, J. Troppmair, R. Benz, U. R. Rapp, *BMC Cell Biol.* **2002**, *3*, 14.
[15] M. Linden, G. Karlsson, *Biochem. Biophys. Res. Commun.* **1996**, *218*, 833 – 836.
[16] H. Kusano, S. Shimizu, R. C. Koya, H. Fujita, S. Kamada, N. Kuzumaki, Y. Tsujimoto, *Oncogene* **2000**, *19*, 4807 – 4814.
[17] C. Schwarzer, S. Barnikol-Watanabe, F. P. Thinnes, N. Hilschmann, *Int. J. Biochem. Cell Biol.* **2002**, *34*, 1059 – 1070.
[18] S. Shimizu, M. Narita, Y. Tsujimoto, *Nature* **1999**, *399*, 483 – 487.
[19] M. G. Vander Heiden, N. S. Chandel, X. X. Li, P. T. Schumacker, M. Colombini, C. B. Thompson, *Proc. Natl. Acad. Sci. USA* **2000**, *97*, 4666 – 4671.

[20] E. H. Cheng, T. V. Sheiko, J. K. Fisher, W. J. Craigen, S. J. Korsmeyer, *Science* **2003**, *301*, 513 – 517.
[21] D. Gincel, H. Zaid, V. Shoshan-Barmatz, *Biochem. J.* **2001**, *358*, 147 – 155.
[22] E. Rapizzi, P. Pinton, G. Szabadkai, M. R. Wieckowski, G. Vandecasteele, G. Baird, R. A. Tuft, K. E. Fogarty, R. Rizzuto, *J. Cell Biol.* **2002**, *159*, 613 – 624.
[23] M. Dolder, K. Zeth, P. Tittmann, H. Gross, W. Welte, T. Wallimann, *J. Struct. Biol.* **1999**, *127*, 64 – 71.
[24] X. W. Guo, C. A. Mannella, *Biophys. J.* **1993**, *64*, 545 – 549.
[25] E. Blachly-Dyson, S. Z. Peng, M. Colombini, M. Forte, *Science* **1990**, *247*, 1233 – 1236.
[26] V. De Pinto, G. Prezioso, F. Thinnes, T. A. Link, F. Palmieri, *Biochemistry* **1991**, *30*, 10191 – 10200.
[27] L. Thomas, E. Blachly-Dyson, M. Colombini, M. Forte, *Proc. Natl. Acad. Sci. USA* **1993**, *90*, 5446 – 5449.
[28] G. Rauch, O. Moran, *Biochem. Biophys. Res. Commun.* **1994**, *200*, 908 – 915.
[29] J. Song, C. Midson, E. Blachly-Dyson, M. Forte, M. Colombini, *J. Biol. Chem.* **1998**, *273*, 24406 – 24413.
[30] R. Casadio, I. Jacoboni, A. Messina, V. De Pinto, *FEBS Lett.* **2002**, *520*, 1 – 7.
[31] G. E. Schulz, *Curr. Opin. Struct. Biol.* **1996**, *6*, 485 – 490.
[32] G. E. Schulz, *Curr. Opin. Struct. Biol.* **2000**, *10*, 443 – 447.
[33] C. A. Mannella, *J. Bioenerg. Biomembr.* **1997**, *29*, 525 – 531.
[34] S. Stanley, J. A. Dias, D. D'Arcangelis, C. Mannella, *J. Biol. Chem.* **1995**, *270*, 16694 – 16700.
[35] M. Colombini, C. L. Yeung, J. Tung, T. König, *Biochim. Biophys. Acta* **1987**, *905*, 279 – 286.
[36] H. Kayser, H. D. Kratzin, F. P. Thinnes, H. Götz, W. E. Schmidt, K. Eckart, N. Hilschmann, *Biol. Chem. Hoppe-Seyler* **1989**, *370*, 1265 – 1278.
[37] N. R. Kallenbach, P. C. Lyu, Z. Honxing in *Circular Dichroism and the Conformational Analysis of Biomolecules* (Ed.: G. D. Fasman), Plenum, New York, **1996**, pp. 201 – 259.
[38] G. Holzwarth, P. Doty, *J. Am. Chem. Soc.* **1965**, *87*, 218 – 228.
[39] M. E. Holtzer, A. Holtzer, *Biopolymers* **1992**, *32*, 1589 – 1591.
[40] J. M. Scholtz, R. L. Baldwin in *Peptides, Synthesis Structures, and Application* (Ed.: B. Gutte) Academic Press, London, **1995**, pp. 171 – 192.
[41] J. M. Scholtz, S. Marqusee, R. L. Baldwin, E. J. York J. M. Stewart, M. Santoro, D. W. Bolen, *Proc. Natl. Acad. Sci. USA* **1991**, *88*, 2854 – 2858.
[42] M. San Miguel, R. Marrington, P. M. Rodger, A. Rodger, C. Robinson, *Eur. J. Biochem.* **2003**, *270*, 3345 – 3352.
[43] K. Wüthrich, *NMR of Proteins and Nucleic Acid*, Wiley Interscience, New York, **1986**.
[44] G. W. Buchko, A. Rozek, Q. Zhong, R. J. Cushley, *Pept. Res.* **1995**, *8*, 86 – 94.
[45] G. D. Henry, B. D. Sykes, *Methods Enzymol.* **1994**, *239*, 515 – 535.
[46] D. S. Wishart, C. G. Bigam, A. Holm, R. S. Hodges, B. D. Sykes, *J. Biomol. NMR* **1995**, *5*, 67 – 81.
[47] J. M. Sanderson, *Org. Biomol. Chem.* **2005**, *3*, 201 – 212.
[48] P. J. Flory, *Science* **1975**, *188*, 1268 – 1276.
[49] D. Grasso, D. Milardi, V. Guantieri, C. La Rosa, E. Rizzarelli, *New J. Chem.* **2003**, *27*, 359 – 364.
[50] T. Mizushima, Y. Ishikawa, E. Obana, M. Hase, T. Kubota, T. Katayama, T. Kunitake, E. Watanabe, K. Sekimizu, *J. Biol. Chem.* **1996**, *271*, 3633 – 3638.
[51] H. Zaid, S. Abu-Hamad, A. Israelson, I. Nathan, V. Shoshan-Barmatz, *Cell Death Differ.* **2005**, *12*, 751 – 760.
[52] N. Borgese, I. Gazzoni, M. Barberi, S. Colombo, E. Pedrazzinni, *Mol. Biol. Cell* **2001**, *12*, 2482 – 2496.
[53] X. W. Guo, P. R. Smith, B. Cognon, D. D'Arcangelis, E. Dolginova, C. A. Mannella, *J. Struct. Biol.* **1995**, *114*, 41 – 59.
[54] R. M. Brito, W. L. Vaz, *Anal. Biochem.* **1986**, *152*, 250 – 255.
[55] D. Babel, W. Götz, H. Götz, F. P. Thinnes, L. Jürgens, U. König, N. Hilschmann, *Biol. Chem. Hoppe-Seyler* **1991**, *372*, 1027 – 1034.
[56] M. Colombini, E. Blachly-Dyson, M. Forte, *Ion Channels* **1996**, *4*, 169 – 202.
[57] M. Y. Liu, M. Colombini, *Biochim. Biophys. Acta* **1992**, *1098*, 255 – 260.
[58] B. Popp, D. A. Court, R. Benz, W. Neupert, R. Lill, *J. Biol. Chem.* **1996**, *271*, 13593 – 13599.
[59] D. A. Koppel, K. W. Kinnally, P. Masters, M. Forte, E. Blachly-Dyson C. A. Mannella, *J. Biol. Chem.* **1998**, *273*, 13794 – 13800.
[60] H. Abrecht, E. Goormaghtigh, J. M. Ruysschaert, F. Homble, *J. Biol. Chem.* **2000**, *275*, 40992 – 40999.
[61] S. A. Paschen, W. Neupert, D. Rapaport, *Trends Biochem. Sci.* **2005**, *30*, 575 – 582.
[62] R. Zalk, A. Israelson, E. S. Garty, H. Azoulay-Zohar, V. Shoshan-Barmatz, *Biochem. J.* **2005**, *386*, 73 – 83.
[63] G. C. Chen, J. T. Yang, *Anal. Lett.* **1977**, *10*, 1195 – 1207.
[64] P. Luo, R. L. Baldwin, *Biochemistry* **1997**, *36*, 8413 – 8421.
[65] C. A. Rohl, R. L. Baldwin, *Biochemistry* **1997**, *36*, 8435 – 8442.
[66] M. Rance, O. W. Sørensen, G. Bodenhausen, G. Wagner, R. R. Ernst, K. Wüthrich, *Biochem. Biophys. Res. Commun.* **1983**, *117*, 479 – 485.
[67] A. Bax, D. G. Davis, *J. Magn. Reson.* **1985**, *65*, 355 – 360.
[68] A. Bax, D. G. Davis, *J. Magn. Reson.* **1985**, *63*, 207 – 213.
[69] J. Jeener, B. H. Meier, P. Bachmann, R. R. Ernst, *J. Chem. Phys.* **1979**, *71*, 4546 – 4553.
[70] J. N. Demas, A. W. Adamson, *J. Am. Chem. Soc.* **1973**, *95*, 5159 – 5168.
[71] L. D. Mayer, M. J. Hope, P. R. Cullis, A. S. Janoff, *Biochim. Biophys. Acta* **1985**, *817*, 193 – 196.
[72] D. Grasso, D. Milardi, C. La Rosa, E. Rizzarelli, *New J. Chem.* **2001**, *25*, 1543 – 1548.

Received: January 8, 2007
Published online on March 23, 2007

